E-ELT M4 adaptive unit final design and construction: a progress report

Biasi, Roberto, Manetti, Mauro, Andrighettoni, Mario, Angerer, Gerald, Pescoller, Dietrich, et al.

Roberto Biasi, Mauro Manetti, Mario Andrighettoni, Gerald Angerer, Dietrich Pescoller, Christian Patauner, Daniele Gallieni, Matteo Tintori, Marco Mantegazza, Pierluigi Fumi, Paolo Lazzarini, Runa Briguglio, Marco Xompero, Giorgio Pariani, Armando Riccardi, Elise Vernet, Lorenzo Pettazzi, Paul Lilley, Marc Cayrel, "E-ELT M4 adaptive unit final design and construction: a progress report," Proc. SPIE 9909, Adaptive Optics Systems V, 99097Y (27 July 2016); doi: 10.1117/12.2234735

Event: SPIE Astronomical Telescopes + Instrumentation, 2016, Edinburgh, United Kingdom

E-ELT M4 adaptive unit final design and construction: a progress report

Roberto Biasi*[a], Mauro Manetti[a], Mario Andrighettoni[a], Gerald Angerer[a], Dietrich Pescoller[a], Christian Patauner[a], Daniele Gallieni[b], Matteo Tintori[b], Marco Mantegazza[b], Pierluigi Fumi[b], Paolo Lazzarini[b], Runa Briguglio[c], Marxo Xompero[c], Giorgio Pariani[d], Armando Riccardi[c], Elise Vernet[e], Lorenzo Pettazzi[e], Paul Lilley[e], Marc Cayrel[e]

[a]Microgate Srl, via Stradivari, 4, 39100 Bolzano-Bozen (BZ), Italy; [b]A.D.S. International Srl, via Roma, 87, 23868 Valmadrera (LC), Italy; [c]INAF-Osservatorio Astrofisico di Arcetri, Largo Enrico Fermi, 5, 50125 Firenze (FI), Italy; [d]INAF-Osservatorio Astronomico di Brera, via E.Bianchi, 46, 23807 Merate (LC), Italy; [e]ESO, Karl-Schwarzschild-Str. 2, 85748 Garching bei München, Germany

ABSTRACT

The E-ELT M4 adaptive unit is a fundamental part of the E-ELT: it provides the facility level adaptive optics correction that compensates the wavefront distortion induced by atmospheric turbulence and partially corrects the structural deformations caused by wind. The unit is based on the contactless, voice-coil technology already successfully deployed on several large adaptive mirrors, like the LBT, Magellan and VLT adaptive secondary mirrors. It features a 2.4m diameter flat mirror, controlled by 5316 actuators and divided in six segments. The reference structure is monolithic and the co-phasing between the segments is guaranteed by the contactless embedded metrology. The mirror correction commands are usually transferred as modal amplitudes, that are checked by the M4 controller through a smart real-time algorithm that is capable to handle saturation effects. A large hexapod provides the fine positioning of the unit, while a rotational mechanism allows switching between the two Nasmyth foci.

The unit has entered the final design and construction phase in July 2015, after an advanced preliminary design. The final design review is planned for fall 2017; thereafter, the unit will enter the construction and test phase. Acceptance in Europe after full optical calibration is planned for 2022, while the delivery to Cerro Armazones will occur in 2023.

Even if the fundamental concept has remained unchanged with respect to the other contactless large deformable mirrors, the specific requirements of the E-ELT unit posed new design challenges that required very peculiar solutions. Therefore, a significant part of the design phase has been focused on the validation of the new aspects, based on analysis, numerical simulations and experimental tests. Several experimental tests have been executed on the Demonstration Prototype, which is the 222 actuators prototype developed in the frame of the advanced preliminary design.

We present the main project phases, the current design status and the most relevant results achieved by the validation tests.

Keywords: ELT, adaptive optics, deformable mirror

1. INTRODUCTION

1.1 Current status of the project

In June 2015 ESO has assigned the contract for the Final Design and Construction of the E-ELT M4 Unit to AdOptica, a consortium of Microgate and A.D.S. International. The contract covers the full design, manufacturing, testing, calibration, transport and re-integration in Chile, which is planned for mid 2023. INAF (Arcetri and Milano-Brera observatories) is subcontracted for the AO scientific advisory and to support the optical tests. Mersen Boostec will furnish the SiC Reference Body. The thin mirror shells will be manufactured by Safran-Reosc and procured directly by ESO.

Adaptive Optics Systems V, edited by Enrico Marchetti, Laird M. Close, Jean-Pierre Véran, Proc. of SPIE Vol. 9909, 99097Y
 · doi: 10.1117/12.2234735

The next major milestone in the project is the Final Design Review, planned for July 2017. The final design activity can be considered a consolidation of the advanced design level already achieved in the preliminary phase, in which some of the key components, in particular the embedded control system, were already developed and tested on a dedicated Demonstration Prototype with 222 actuation points, the E-ELT M4DP [1]. Part of the design activity conducted so far has been dedicated to the assessment of some particularly challenging performance requirement for the M4 unit. The present paper is focused on the description of such validation tests and analysis. Three main aspects are addressed:

- the adaptive optics temporal error verification through simulation, which also implies:
    - the experimental identification of the E-ELT M4DP transfer function matrix;
    - the verification of the low modal cross-coupling achievable by the system;
    - the assessment of the *global control* computational time and data transfer latency;
- the E-ELT M4 long-term stability, which is expressed as a strict requirement on the system planarity over a time window of 15 days and considering a temperature variation of 6°C; this is one of the most challenging aspects of the project, which mainly affects the capacitive sensor design; the experimental verification of the sensor performance through an ad hoc experimental specimen will be presented;
- the new expansion gas cooling concept, showing and explaining the evolution of the deformable mirror cooling design, which should highly improve the system reliability and efficiency; an experimental tests together with a numerical simulator are presented, whose main role is a preliminary validation of the new concept.

2. AO RESIDUAL TEMPORAL ERROR

The M4 adaptive unit is a fundamental part of the AO system of the E-ELT and as such it can be considered as enabling technology for the achievement of the E-ELT scientific goals. It must guarantee static and dynamic performance in the correction of optical aberrations. Several important requirements must be addressed by the system. This section is focused on the analysis, which provides evidences of the E-ELT M4DP following error performance, evaluated through a simplified simulation of the adaptive optics loop. The assessment of this requirement involves the description of the deformable mirror dynamics, which is provided by the experimental identification of the system modal transfer function matrix, Section 2.1. The transfer function matrix also allows to verify the low modal entanglement of the deformable mirror. A low modal cross-coupling is explicitly required by ESO, and it is also a hypothesis at the base of the residual temporal error verification. The evaluation of feedforward computational time and data transfer delay are addressed in Section 2.2 and are necessary parameters to model the optical loop. The numerical simulation of the adaptive optics loop and the residual temporal error performance of the system are shown in Section 2.3.

2.1 DP transfer function identification

The purpose of this experimental activity is the identification of the E-ELT M4DP modal transfer function matrix (111x111 size for each one of the two prototype mirrors [1]), from modal shape commands to measured shape. The identification has been done through the Welch's averaged periodogram method, an improvement of the straightforward calculation as the ratio of the output/input Fast Fourier Transform. The input is here represented by the command time history, which is applied at the system maximum command rate, i.e. 1kHz. The feedforward and feedback control parameters and gains are left unchanged with respect to the operational condition settings, so that the identified transfer function is fully representative of the system in a typical working condition. Each i^{th} column of the transfer function matrix has been obtained through the system excitation with a command time history, whose spatial deformation has been set equal to the i^{th} modal shape, modulated in time as a pink Gaussian noise to obtain a frequency content in the range 0-1kHz. The noise standard deviation has been tuned to satisfy safety and hardware constraints, in terms of both maximum force available and maximum deformation/displacement achievable. The measurement output has been acquired through the capacitive sensors. The final useful frequency bandwidth of the identified transfer function is about 1 kHz. The identification bandwidth is limited by the impossibility to appropriately excite higher frequencies. A higher excitation bandwidth cannot be achieved because of the constraint on the maximum command rate of the system, 1 kHz. This limitation is shown in Figure 1, where it is shown the Fast Fourier Transform of the modal excitation signal used to identify the column 60 of the

transfer function matrix, together with the Fast Fourier Transform of the system modal response. It is evident that the useful frequency range excited is a little bit lower than 1kHz, where the excitation approaches the null value.

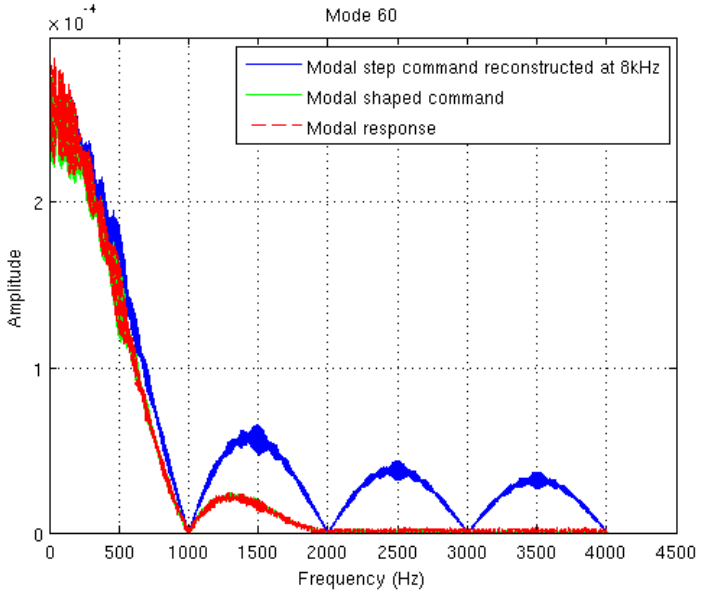

Figure 1. Comparison of the FFT of an input excitation signal sampled through 1 kHz pure step commands (solid blue), with the very same time history pre-shaped by the M4DP control system (solid green) and the measured mirror modal response (dashed red).

The bode diagram of all the transfer functions placed on the diagonal of the identified matrix is shown by Figure 2. As already pointed out, the transfer functions can be correctly evaluated in the frequency range 0-1kHz. Moreover, the last 10 modal shapes are quite inaccurate because of the system limitation in maximum force, which prevents the possibility to obtain a good signal to noise ratio.

The identified E-ELT M4DP transfer function matrix easily allows verifying the system modal cross coupling. Robust stability and performance of the AO loop requires a well behaved dynamic response of the M4 unit. In particular, assuming AO control is based on static inversion, moderate modal cross couplings in a frequency range below twice the expected AO loop cross-over frequency is required to ensure appropriate robustness margins. The ESO requirement refers to the optical modal shapes defined over the surface of the whole unit, but on the M4DP it is not possible to work with this modal basis because of the reduced number of actuation points. This is the reason why the modal cross-coupling is here assessed for the electro-mechanical modal basis, i.e. the right singular vectors of the static feedforward matrix [2]. Figure 3 shows the modal cross-coupling of the electro-mechanical modal shapes number 1 and 20 with respect to the first twenty electro-mechanical modal shapes. Figure 4 summarizes the maximum modal cross coupling in the frequency range 0-100 Hz, within the first 20 modal shapes. This modal cross-coupling is required to be lower than 5%, this constraint is satisfied with a good safety margin by the system.

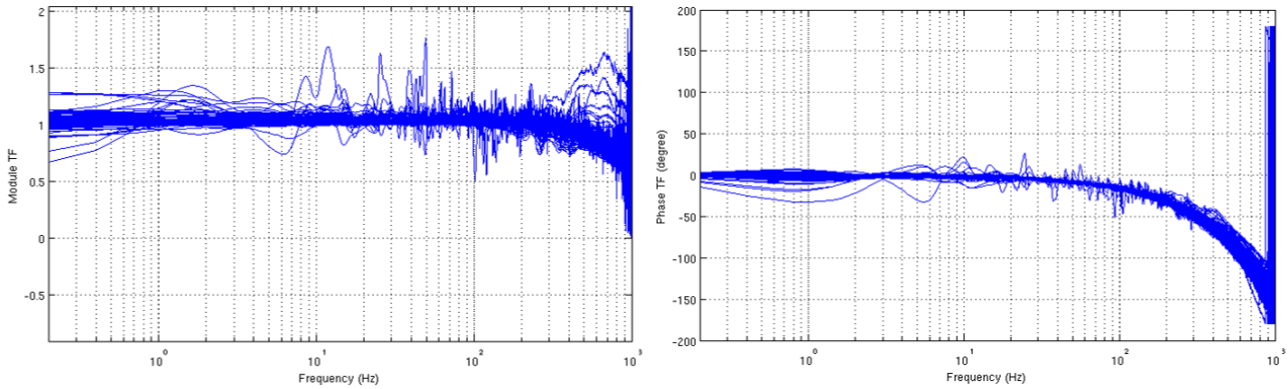

Figure 2. Bode diagram of the M4DP diagonal transfer functions.

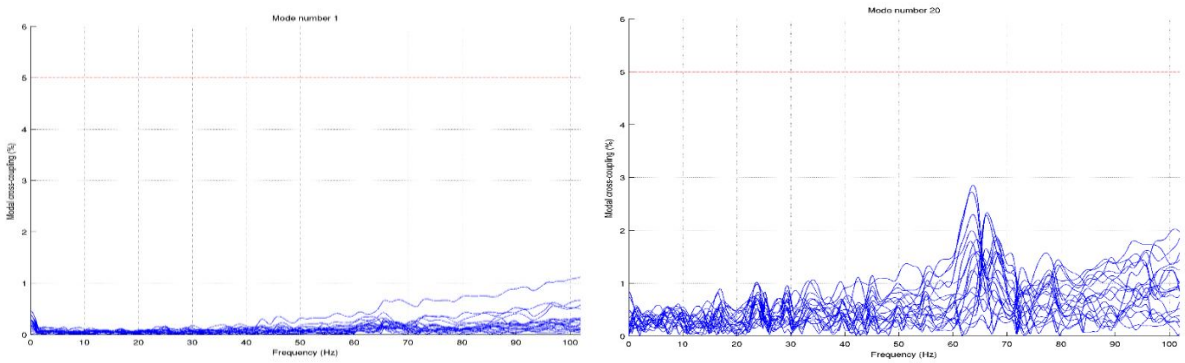

Figure 3. Modal cross coupling verification within the range 0-100 Hz, for the modal shapes number 1 and 20. The dotted red line represents the limit of 5% imposed by ESO requirement.

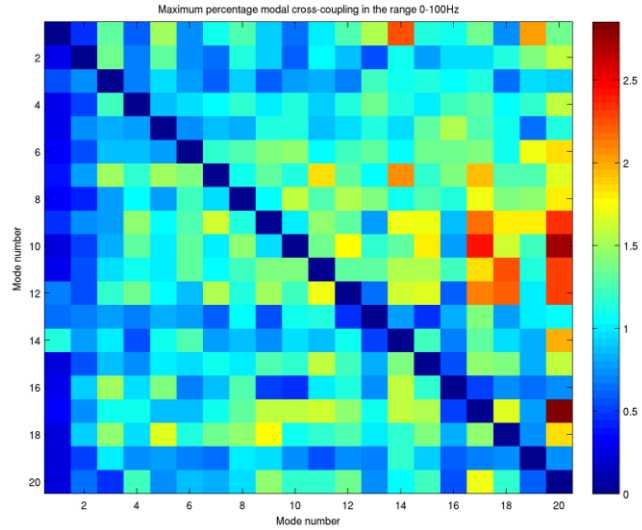

Figure 4. Maximum modal cross coupling percentage in the range 0-100 Hz, within the first 20 electro-mechanical modal shapes.

2.2 Local control and deterministic network latency test

The control architecture of the M4 mirror comprehends a co-located actuator control loop and a global control action based on a force feedforward strategy [2]. The actuator loop is implemented in the embedded control system, while an external computing unit, named *local control unit* and based on workstations and hardware accelerators, performs the computations

related to the feedforward action. Another fundamental task performed by the *local control* is the saturation management. The telescope Deterministic Network sends M4 commands either as local actuator position setpoints or as modal amplitudes of an optical modal base. In both cases, the saturation management determines if the commanded actuator position and force patterns are within a safe operational range for the mirror. When actuators commands are sent, an out-of-range frame can be only skipped, keeping the mirror in its previous position; conversely, when the mirror is commanded through modes, the number of applied modal shapes can be reduced to bring the force pattern within the acceptable range. Such adaptive modal control is performed autonomously and in real-time by the *saturation management box*. All these global tasks pose a significant challenge in terms of computational throughput and determinism. Therefore, already during the design phase, we planned with ESO to carry out dedicated tests in which we measure the performance of the whole communication and computational chain and refine progressively the interface protocols. In the tests conducted so far we achieved the goal of commanding the Demonstration Prototype (222 actuators) through the deterministic interface and with a full implementation of the *local control*, including saturation management. The measured computational latency of 118μs allowed confirming the estimated value of 278μs for the final M4 implementation.

2.3 Numerical simulation of the AO loop

The present analysis is a simplified numerical simulation of the adaptive optics loop, whose assumptions and directions have been provided by ESO to assess the system performance in terms of residual wave-front error. It is important to remark that these results do not consider the fitting-error and the super-Nyquist error. The requirement linked to the present numerical simulation is verified on the E-ELT M4DP because the present analysis exploits the M4DP identified transfer function matrix.
The main components of the adaptive optics loop modeled are:

- the wave front sensor, the A/D converter, the mirror shape reconstructor and the actuator command generator, which are modeled as pure time delays, through their latencies; the overall latency is defined in the measure of two adaptive optics loop samples;
- the computation delay of the command saturation, mirror zonal setpoints and feedforward force (see Section 2.2);
- the integral digital controller of the adaptive optics loop, whose modal gain is defined on the basis of the loop sampling frequency;
- the deformable mirror response, which is defined through the identified E-ELT M4DP modal transfer function (see Section 2.1).

The simplified simulation model is sketched in Figure 5; the input/output of all the blocks are expressed in modal space. In principle the optical modal basis should be used for this test, but with the M4DP the electro-mechanical modal basis (right singular vectors of static feedforward matrix) is mandatory to allow the transformation from actuator space to modal space. However, this choice should not affect the simulation results because the integral controller gain is the same for all modal shapes. The turbulence time history contains the following optical aberrations: the median seeing temporal error (outer scale 50m, 0.85''@ λ=0.5μm), the telescope focus disturbance, the telescope x-y astigmatism disturbance, the telescope x-y coma disturbance. The deformable mirror response is obtained through the M4DP identified modal transfer function matrix; the M4DP transfer function matrix is approximated as diagonal, i.e. the modal cross coupling is considered negligible. This approximation is acceptable because the mirror wave front error is dominated by the contribution of low spatial frequency modes at low frequency, whose cross coupling is required to be negligible, as assessed in Section 2.1. Moreover, the transfer function confirms the presence of a good modal decoupling for most of the considered modal shapes, over a consistent low frequency range. The diagonal elements of the identified transfer function matrix have been converted from frequency domain to Laplace domain by fitting them with polynomial transfer functions characterized by 2 zeros and 3 poles for each modal shape. The choice of the zeros and poles number have been triggered by a tradeoff between accuracy and numerical issues linked to the fitting of high order polynomials. The transfer functions in Laplace domain have been transformed in state space, so that a time domain simulation of the mirror modal response can be performed and the deformable mirror contribution to the adaptive optics loop computed.

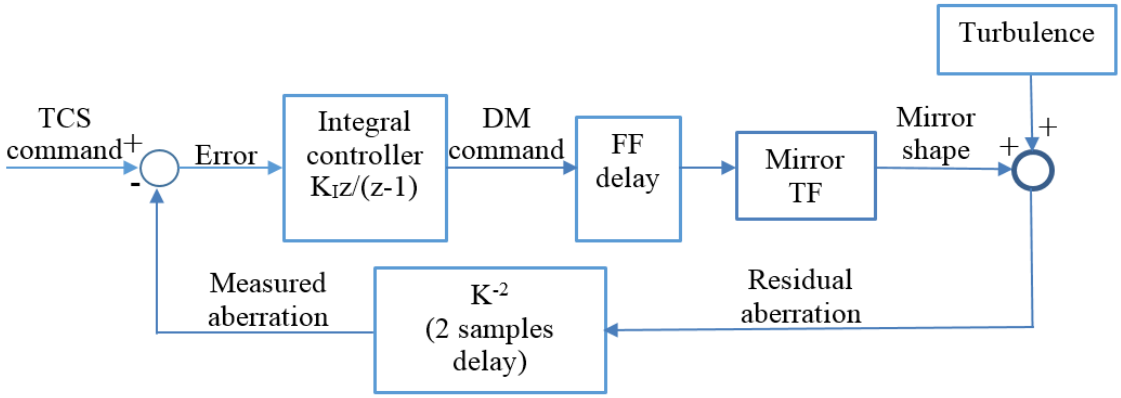

Figure 5. Sketch of the AO loop simplified model exploited for the present simulation.

Figure 6 shows the simulation results of the modal shape number 5 with a sampling frequency of the optical loop equal to 1000Hz. The green curve represents the turbulence time history (@1kHz), the blue curve is the command received by the deformable mirror (@1kHz), the black curve is the high frequency mirror step command (@80kHz), the magenta curve is the high frequency mirror modal response (@80kHz), the red curve is the average position reached by the mirror during the command step, which represents the output of the deformable mirror block (@1kHz). The residual aberrations, i.e. the wave-front error rms, are computed as the sum between the deformable mirror output, i.e. the average compensation introduced by the mirror, and the average turbulence over the command step.
The wave front error is required to be computed for three different sampling frequencies of the adaptive optics loop: 500Hz, 700Hz and 1000Hz. The simulation results, together with the limit wave front error required by ESO, are reported in Table 1. The results are fully compliant with the specifications.

Table 1. Wave front error when the AO loop works with a sampling frequency of 1000Hz, 700Hz and 500Hz.

AO sampling frequency	AO controller integral gain	Wave-front error limit	Wave-front error simulated
500 Hz	0.375	100 nm	99.6 nm
700 Hz	0.35	78 nm	74.6 nm
1000 Hz	0.325	60 nm	55.5 nm

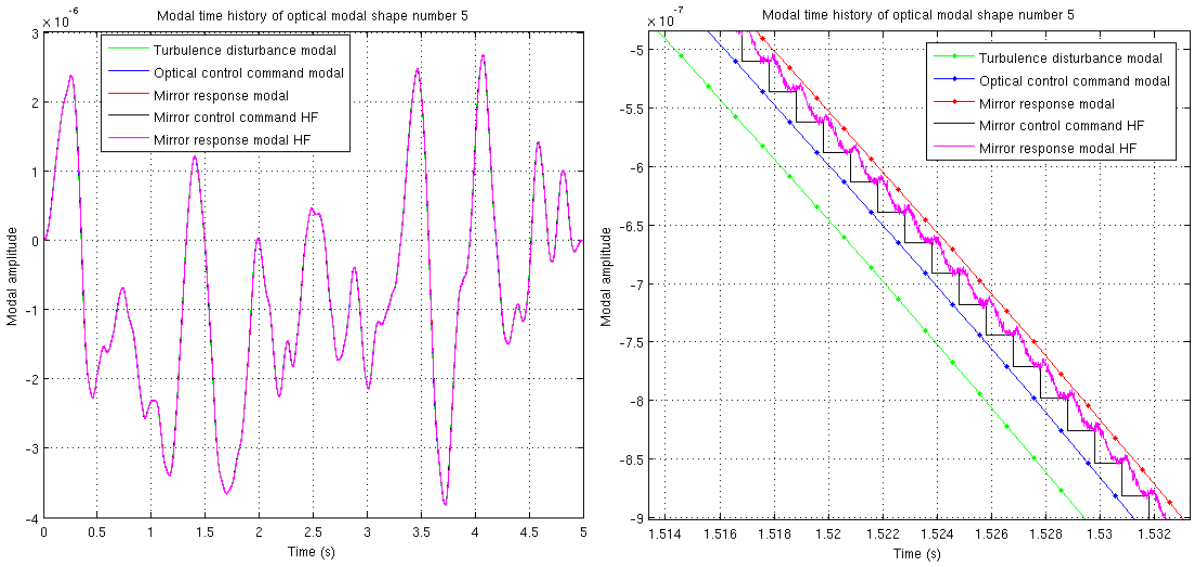

Figure 6. Modal shape number 5 simulated response, AO loop sampling frequency set at 1000 Hz: left, full time history, right, zoomed view.

3. LONG-TERM STABILITY

Long term stability requirements are set for the M4 shape to constrain the creation of scalloping in the telescope pupil. The deformable mirror long-term stability and segments co-phasing is one of the main challenging aspects of the E-ELT M4 unit design. The mirror, which is composed by six independent segments (petals) must guarantee a very strict planarity of the complete reflecting surface, through the definition of a limit local curvature (20km radius over 80mm of spatial scale or larger). This specification must be satisfied for a period of at least 15 days and a maximum temperature variation of 6°C. It is worth noticing that this requirement remains unchanged also when the mirror is working in open optical loop, i.e. without any optical feedback about its own deformation.

3.1 Contact concept and test validation

The design of the capacitive sensor connector, which provides the electrical link between the metalized armature placed on the reference body and the electronic board, is a critical component. The connection must guarantee:

- a stable and reliable electric contact in presence of low currents;
- low and linear forces and torques exchanged between the reference body and the electronic board.

Both these points are of primary importance to assure the system long-term stability, the first one for a correct and stable electrical connection, the second one to guarantee a good mechanical decoupling between the different system components without hysteresis. To obtain this, we introduced a novel connection based on a magnetic retention system. This provides at same time a stable, low resistance path between the capacitive sensor armature and the signal conditioning electronics and very weak and linear, hysteresis-free force transmission between the reference body, where the sensor armatures are placed, and the brick structure hosting the electronics. The contacts are all redundant to increase furthermore the reliability. This solution improves also significantly the system maintainability, in fact all contacts mate/unmate automatically and reliably each time the control brick is installed/uninstalled, without requiring any specific intervention or check by the operator.

Figure 7 shows the experimental setup exploited to verify the capacitive sensor armature connector robustness, i.e. good electrical contact quality and stability, with respect to possible relative movements between the brick and the reference body and/or brick mounting tolerances.

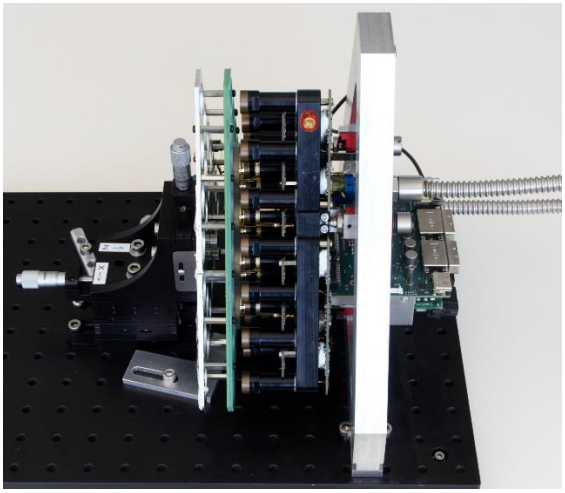

Figure 7. Test setup for the validation of the armature connector robustness with respect to mounting tolerances and relative movements between the brick and the reference body.

3.2 Capacitive sensor stability

The capacitive sensor thermal stability is a key aspect of the E-ELT M4 design, because it can potentially have a high impact over the system long-term stability. This is the reason why a specific test campaign has been performed to assess accurately the achievable performance. This test required the development of an ad hoc specimen, the breadboard number 5 (BB5). The BB5 is shown in Figure 8 and it has been designed to address both the electro-mechanical interface for the capacitive sensor armature (see Section 3.1) and the sensor electronics. Four main parts compose the breadboard:

- a plate realized in SiC material, which is representative of the final unit reference body;
- the capacitive sensor armature connectors that provide the electro-mechanical interface between the metalized area of each capacitive sensor and the electronic board;
- the capacitive sensor electronic board with a serial interface for ADC readout;
- a thick Clearceram-Z mirror with a coated face, laying over the reference body through three shims, which should provide an ideal isostatic support; on the mirror coating is injected the reference signal required for the capacitive sensor functioning.

The capacitive sensor board is capable to perform the readout of 28 sensor channels; 10 sensors measure the air gap between the reference body and the mirror, while the remaining 18 channels measure the capacitance of 18 fixed solid state capacitors. These channels act as reference and operate in an ‘electronic only’ mode in which the air gap capacitance is substituted by fixed capacitors with ±30ppm temperature coefficient. The role of the channels connected to the reference capacitors is useful during test to understand the ‘electronic only’ performance of the sensing system; this kind of solution is also useful in providing a reference to compensate the pure electronic drift of the sensors due to temperature and humidity.

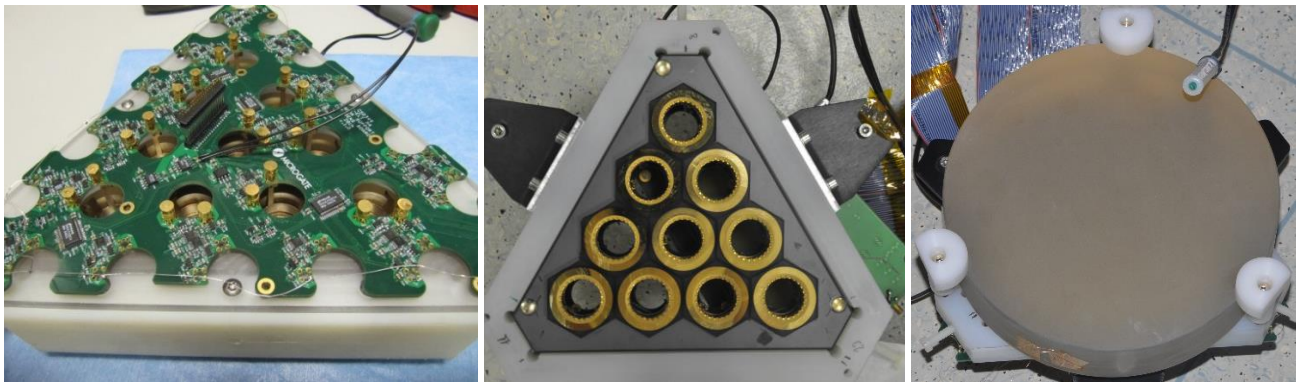

Figure 8. BB5 electronic board (left), SiC reference body with metalized tiles (center), coated Clearceram-Z mirror (right).

The first test aims to verify the capacitive sensor thermal stability of the 'electronics only' design, plus the armature connector interface, without the need of the mirror. After removing the drift of the common piston mode, which does not affect the system performance, the measured stability is of the order of ±1bit/°C, corresponding to about 2 nm/°C. These results are completely consistent with the ones obtained removing the capacitive sensor connectors, confirming that the impact of inserts and magnetic contacts is negligible.

The final test verifies the capacitive sensor thermal stability when a real air gap between the mirror and the reference body is measured. The temperature profile applied during test is reported in Figure 9. Two effects dominate the capacitive sensor drift with temperature:

- the piston, mainly induced by the different expansion between the mirror shims and the borosilicate tiles;
- the focus, mainly induced by the different thermal expansion between the borosilicate tiles and the SiC reference body and the effect due to the in plane forces generated by the shims, because of the differential thermal expansion between reference body and mirror.

The piston due to shims expansion can be removed because not present on the final system, where there is only the effect of the tiles expansion. However, as already stated, a common piston drift does not affect the final system performance, so it is possible to discard it completely. The focus contribution can be purged as well, because Finite Element simulations confirm a negligible entity of this contribution on the final system. It is worth noticing that the modeling procedure of this phenomenon has been experimentally validated thanks to the BB5 prototype. The here presented results also consider the electronic drift compensation based on the 18 reference channels. Figure 10 shows the measurement of capacitive sensors, with rigid motions and focus removed, as function of time (left image) and temperature (right image). It is possible to appreciate a maximum drift of about 0.8 nm/°C.

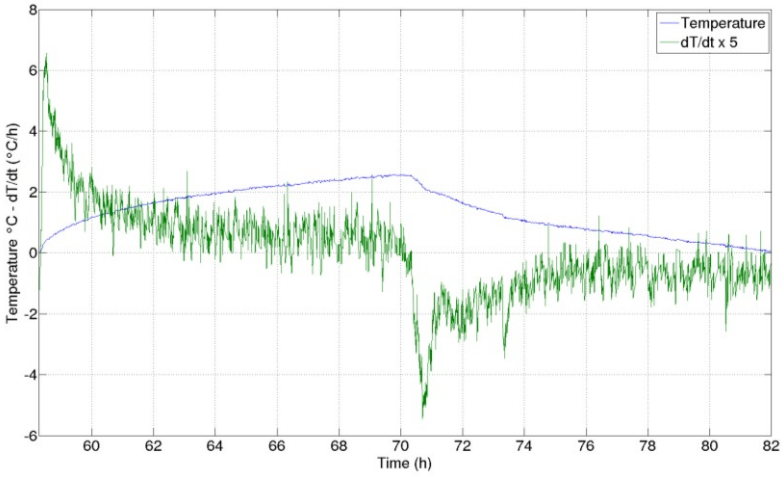

Figure 9. - Temperature and temperature derivative time history.

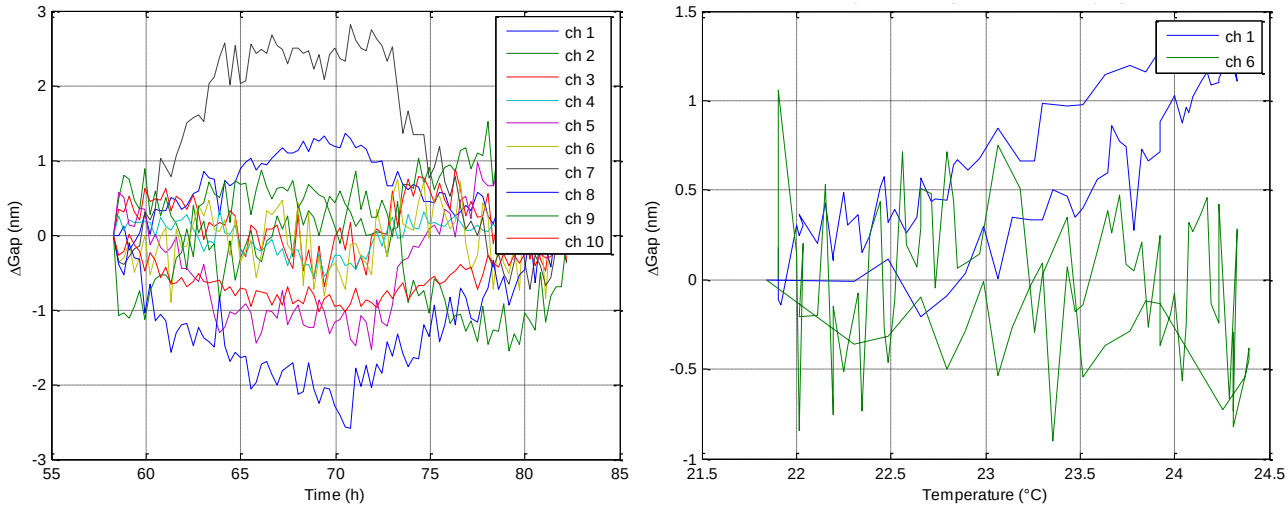

Figure 10. Variation of gap measurements after electrical drift compensation and rigid shell deformation plus focus removal, as function of time (left), and temperature (right).

The humidity variation during the test is recorded. Humidity can affect the measurement of capacitive sensors by changing the air dielectric constant. After computation, the effect of a humidity change on the sensor stability can be considered negligible, so the measurements dependence by humidity can be discarded and no compensation is introduced or foreseen.

4. NEW EXPANSION GAS-COOLING

The position of the M4 unit in the telescope induces stringent requirements in term of thermal uniformity and cooling reliability. Any temperature gradient at the level of the intermediate focal plane creates some aberrations on the optical path and with its position inside the telescope, the risk of liquid leakage on M1, M5 or M3 must be avoided.

The cooling of all previous deformable mirrors is based on glycol flow driven by appropriate hoses and pipes through the system cold plate, which represents the main heatsink of the electronics. This solution, despite successful on the systems developed up to now, has been revised for the E-ELT M4, mainly to improve the system reliability and avoid possible damages to the adaptive unit itself or even to other telescope components in case of glycol leakage. Moreover, the classical concept of the cold plate is no more applicable to the M4 unit, because the electronics is mounted directly on the SiC reference body in a modular way, through the brick concept [1]. All the bricks are connected partly in series (within the same segment) and partly in parallel (between different segments) to the cooling system through hoses to provide the cooling of the electronics mounted on them. These are the reasons why, a new cooling design has been developed , where the concept was to substitute the glycol with a liquefied gas, the R134a refrigerant. The main advantage of this solution is the R134a property to assume the gas state at typical ambient pressure and temperature, so that in case of leakage no relevant damages to the system are caused. A first implementation of this concept to the E-ELT M4DP resulted successful, but the solution was very inefficient with respect to the power consumption required to cool the system. This is the main reason for the introduction of the new expansion gas-cooling concept, which allows reaching a very high efficiency, with the further advantage of a relevant reduction of the refrigerant mass flow rate, about one order of magnitude lower than the glycol baseline solution.

The new expansion gas cooling solution requires for the proper functioning all the typical components of a system based on refrigeration cycle: compressor, condenser, expansion valve, evaporator, pressure control valve (see Figure 11). The plant is designed to handle a thermal load of 9 kW. The compressor and the condenser (called heat exchanger in Figure 11) are placed in the telescope basement, where the condenser has the possibility to be connected to a coolant link provided by the telescope cooling facility. The refrigerant, i.e. R134a, enters the compressor in a pure gas state, after compression the fluid passes through the condenser so that a high pressure liquid refrigerant is obtained. Then a hose with an estimated length of the order of few hundreds of meters drives the refrigerant to the E-ELT M4 unit, which is placed several tens of meters above the compressor. Once reached the unit the refrigerant expands through six expansion valves, positioned at the beginning of six parallel circuits, one for each mirror segments. After expansion the flow is in a two-phase state, i.e.

the fluid boils at a constant temperature while passes through the bricks and the crates of each segment, absorbing heat from the system. In this way the adaptive mirror itself becomes the evaporator. The boiling temperature of the fluid inside the evaporator is set by controlling the evaporator pressure through a single pressure valve. The flow at the evaporator outlet is enforced to be in a gas state (superheated flow) by controlling the six expansion valves placed at the M4 inlet. At the unit outlet a manifold collects all the fluid in gas state and send it back to the pressure valve and to the compressor through the cooling system downlink.

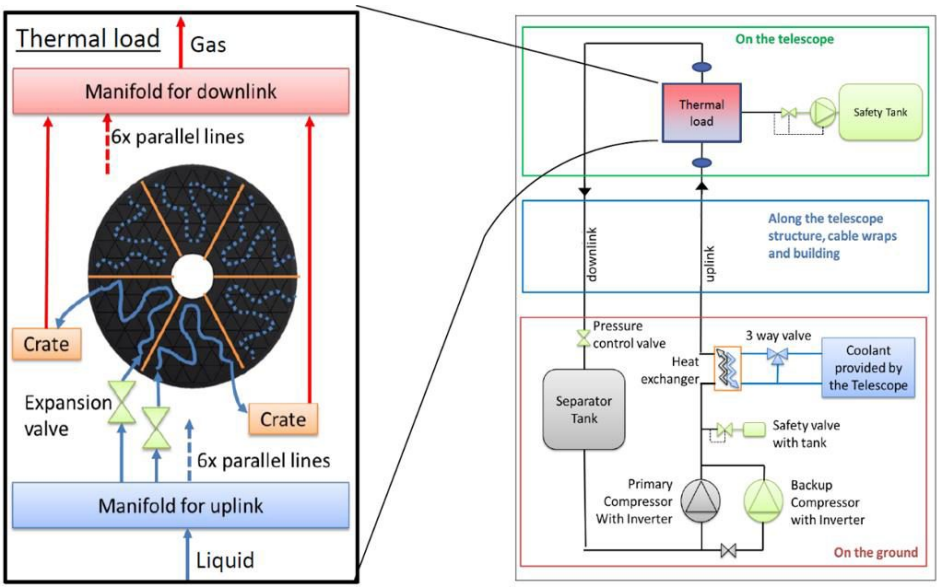

Figure 11. Expansion gas cooling layout of the E-ELT M4.

A usual implementation of the refrigeration cycle works with an ON-OFF compressor control, i.e. the compressor is activated when the temperature exceeds a prescribed upper limit and it is deactivated when the temperature falls below a lower limit. The E-ELT M4 system requires a tight temperature control, so the compressor works in a continuous way. The fluid expansion process and the pressure inside the evaporator always require to be controlled through a feedback loop, and the system performance and robustness in terms of temperature uniformity in time and space is based on an appropriate tuning of the overall control system. The cooling control must guarantee that the adaptive mirror surface tracks the ambient temperature with an accuracy of +0.5/-1°C. The feedback control works by commanding through an integral action the aperture of the six expansion valves placed at the evaporator inlet and the pressure valve. The role of the pressure valve is to maintain the flow pressure inside the evaporator at a specified value, which in turn sets the flow boiling temperature inside the evaporator. In this way it is possible to control the system temperature. On the other side, the aperture of the six expansion valves is commanded to assure that at the end of the evaporator the flow reaches a superheated condition, i.e. the fluid remains in a stable two-phase flow condition through all the evaporator route and just at the end all the fluid is transformed in gas state, thus controlling ultimately the flow rate in each segment.

4.1 Numerical model

The application of a gas expansion cooling system to a secondary adaptive mirror for tight temperature control represents a non-conventional solution, so the capability to have a preliminary assessment of the system performance through a simulator is very appealing. Also because the typical thermal time scale of the problem at hand are in the order of several hours, so the control system tuning and the experimental test execution are usually very time consuming.

The system effectiveness and performance are mainly verified at the evaporator level, which is the sensible element of the system, i.e. the mirror. So, the simulation effort has been focused so far to model the evaporator, together with the expansion valve and the pressure control valve, which can be important in the frame of the feedback control system simulation. The description of the other refrigeration cycle components is lumped in the evaporator boundary conditions,

which are considered sufficiently reliable and stable in the current design, and can be easily gathered/checked from the experimental test measurements too.

The evaporator can be considered part of the more general heat exchanger modeling, so that the same model can be potentially exploited to simulate the evaporator, as well as the condenser, through the introduction of few modifications. However, the present work is focused on the evaporator only. The model is developed introducing the following approximations:

- 1D model, i.e. the fluid properties are supposed to vary only along the flow direction;
- pressure drops inside the evaporator are negligible;
- expansion across the valve is isenthalpic;
- two-phase regions in the evaporator are homogenous;
- the heat exchange between the evaporator and the external ambient through air natural convection is considered negligible.

The modeling is performed through a Finite Volumes discretization of the evaporator domain, approximated as 1-dimensional [3]. The mass and the energy conservation laws for a compressible flow are applied to the R134a refrigerant, discretized through *n* Finite Volume cells. The momentum balance is neglected because pressure drops are not taken into account. Each Finite volume has two unknowns: specific enthalpy, and fluid mass inside the cell. In addition there is the pressure unknown, which is considered constant along the evaporator (constant in space), but it is not stationary, i.e. it changes in time. The boundary conditions are defined as: the evaporator input and output mass flow, the input flow specific enthalpy. The input specific enthalpy can be computed on the base of the flow pressure and temperature at the evaporator inlet, before the expansion valve. The input and output mass flow of the evaporator can be defined as a nonlinear function of the pressure drop across the input and output evaporator valves and the aperture of the valves themselves. Figure 12 summarizes the problem discretization scheme with the above described unknowns. The refrigerant nonlinear constitutive law is managed through the use of ad hoc look-up tables appropriately computed through the use of the coolProp library [4].

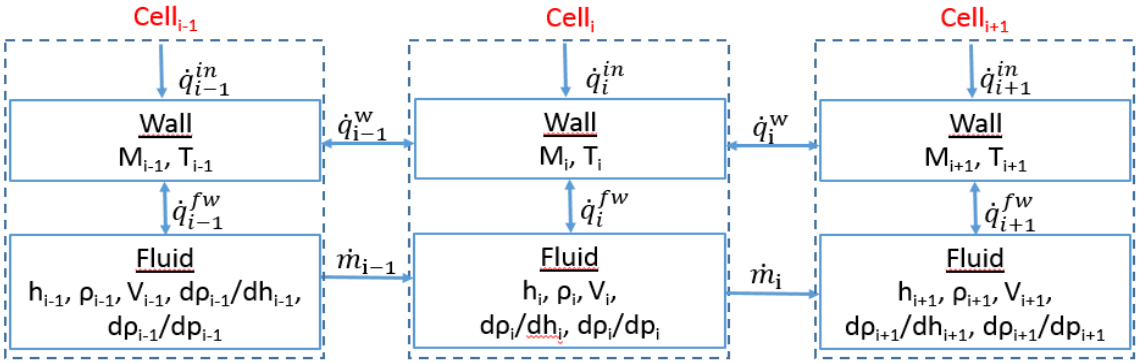

Figure 12. Finite Volumes scheme: specific enthalpy h, density ρ, cell volume V, mass flow $\dot{m}$, wall mass M, wall temperature T, heat fluxes $\dot{q}$.

The evaporator wall is modeled through a thermal mass, which is linked to a temperature unknown and can exchange heat with (see Figure 12):

- the evaporator wall of the previous cell through conduction;
- the evaporator wall of the next cell through conduction;
- the evaporator refrigerant of the same cell through convection;
- an external heat flux defined by the user to model the heat power load introduced by the electronics.

The most critical parameter to be defined is the heat transfer coefficient between the refrigerant and the wall, which is function of several input: refrigerant phase and vapor quality, mass flow, heat flow, system real geometry and components. Several correlations are available in literature, the simulator is now using the Gungor-Winterton formula [5], but a good numerical-experimental matching, see Section 4.2, always requires an experimental tuning of this coefficient.

4.2 Preliminary experimental setup

A preliminary experimental setup useful to validate the new cooling concept, together with the numerical model, has been developed. The setup main components can be summarized as, see also Figure 13:

- a compressor with a condenser located in the basement of the Microgate building;
- a 200m long pipe as uplink, which brings the R134a fluid up to the Microgate laboratory, placed about 25m over the basement level;
- an expansion valve at the evaporator inlet;
- the evaporator, composed by two aluminum shells, also called power plates, mounted in series, through which the fluid is carried through appropriate serpentines, which are capable to introduce a thermal load of about 1kW thanks to electrical resistances;
- 200m long pipe as downlink, which drives back the fluid to the building basement;
- a pressure control valve;
- some pressure and temperature sensors located in several places of the circuit, and exploited for the feedback control and the system monitoring; the expansion valve is controlled by a temperature sensor placed at the evaporator outlet, the evaporator pressure is controlled through a pressure sensor placed before the pressure valve, the compressor is controlled through a pressure sensor placed before the expansion valves.

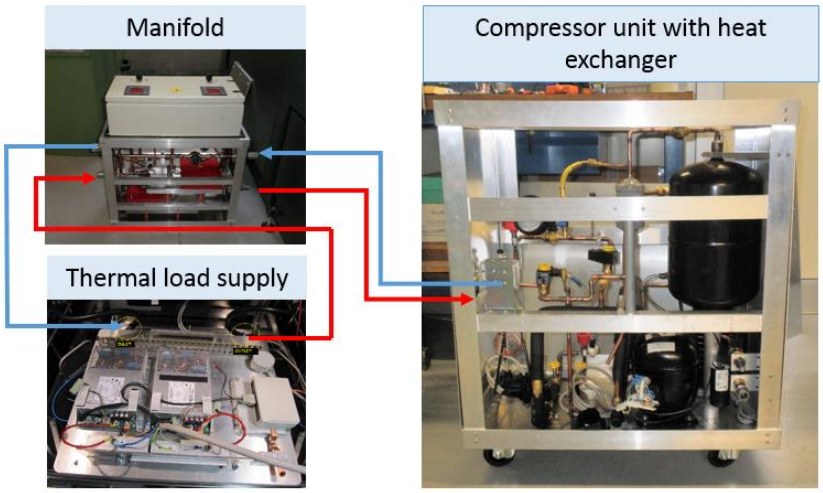

Figure 13. Experimental setup.

Figure 14 shows the cooling system capability to track a reference value of the pressure inside the evaporator (figure on the left), and the capability to set at the evaporator outlet a reference temperature. The cooling system, by controlling these two parameters, can handle the temperature reached by the first power plate. The numerical simulation seems to predict a faster response of the system with respect to the experimental evidences, even if a more accurate simulation of the system dynamics can be observed when a decreasing step is applied at the reference pressure. The reason is still under investigation.

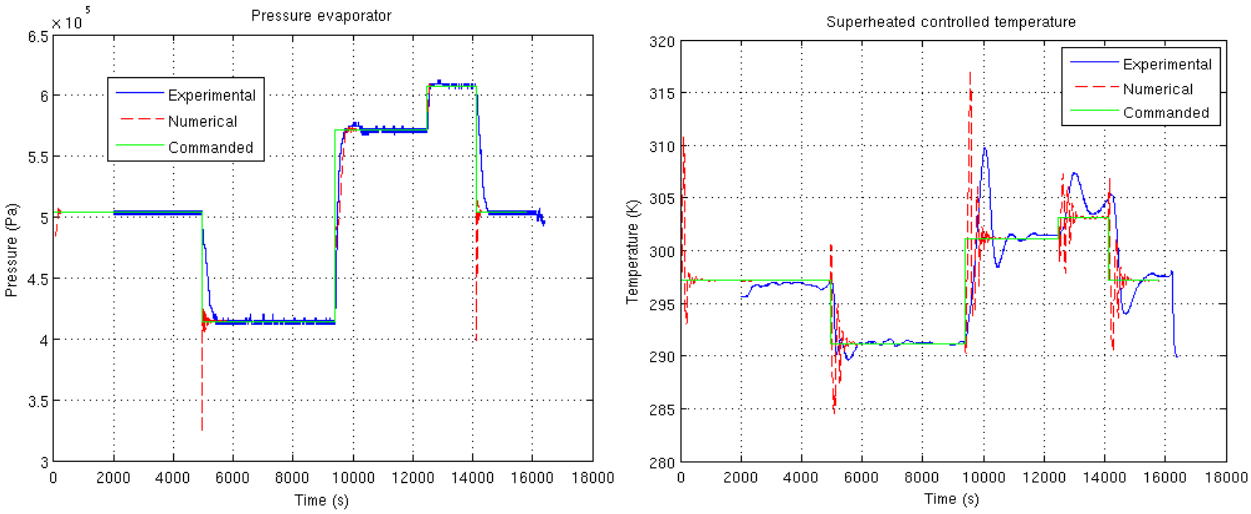

Figure 14. (left) Evaporator pressure control, reference value (green), experimental tracking (blue), numerical tracking (red); (right) controlled temperature at the evaporator outlet, reference value (green), experimental tracking (blue) numerical tracking (red).

Figure 15 shows on the left the temperature measured during test on the first power plate, which represents the sensible element where the temperature needs to be controlled; on the right the temperature time history on the second plate, whose function is to enforce a superheating temperature to the fluid. It is possible to appreciate that step changes of the reference pressure allow to control easily the temperature reached by power plates. The numerical simulation still highlights an overestimation of the system dynamic response when step changes are applied to the reference pressure. The predicted temperature of the power plates is highly dependent on the heat transfer coefficient between the refrigerant and the wall. For the present simulation this parameter is tuned on the base of experimental evidences and kept constant during all the analysis; however, as explained in Section 4.1, a change in the operating condition usually involves a change of the heat transfer coefficient too, which is here neglected for simplicity. This is the reason why the temperature prediction of the simulator is more accurate for some operating conditions and less accurate for others.

On the basis of the experimental results, the new gas cooling system concept seems adequate in terms of cooling capabilities, control system dynamic performances and efficiency. Moreover, the vibrations introduced into the system have been verified to be in-line with the previous solution tested on the E-ELT M4DP during the optical tests, and anyway lower than using a typical water-glycol cooling.

The numerical-experimental correlation can still be improved, however the simulator is already capable to predict with an acceptable accuracy the system behavior and the control system performances, so that it is a very useful tool to obtain a preliminary evaluation of several solutions, both in terms of plant layout and control systems design.

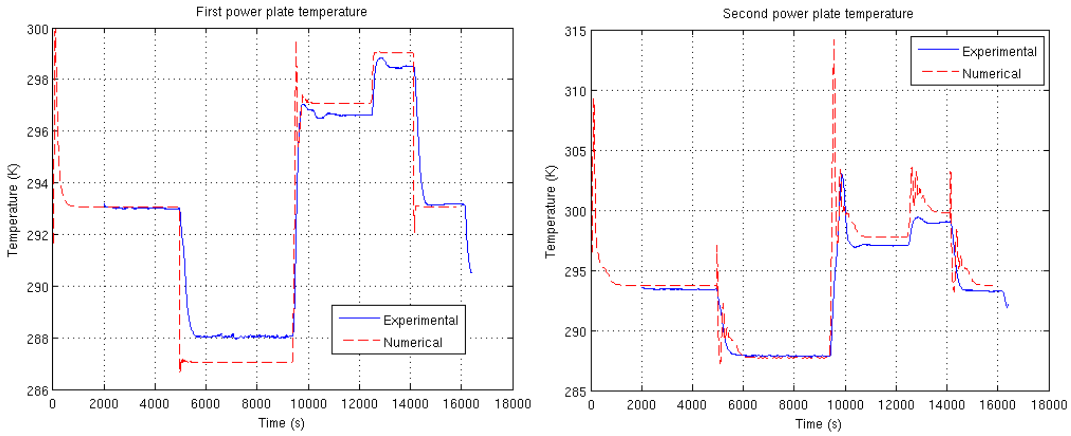

Figure 15. Numerical experimental-correlation of the temperature read by sensor on the first (left figure) and second (right figure) shell of the evaporator.

4.3 Forthcoming improved experimental setup

The next step is to perform a test on an improved experimental setup. The modifications introduced with respect to the setup described in Section 4.2 are:

- the E-ELT M4 DP is connected on the cooling circuit after the first power plate; the first power plate plus the M4DP can reproduce the thermal load of a single M4 unit segment, moreover the M4DP can be rotated around its spin axis to test the cooling efficacy when the system is working at different elevation angles;
- a second evaporator cooling line is added in parallel to the first one, together with a proper independent expansion valve; this cooling line is provided by two appropriate power plates, which can reproduce a thermal load equivalent to the other branch of the evaporator, i.e. equivalent to a single M4 unit segment.

The objectives of this second experimental setup are to verify the capabilities of the new cooling solution in terms of:

- temperature uniformity over the different bricks of the M4DP during a typical operational condition of the mirror prototype;
- required delta temperature between the M4DP external surfaces and the ambient temperature;
- cooling system stability and reliability during long-term test sessions;
- cooling system performance robustness with respect to different elevations of the M4DP to evaluate the impact of changes in the gravity vector orientation.

5. FINAL REMARKS

The present paper highlights some challenging requirements, which must be satisfied by the E-ELT M4 unit. A concise justification of such requirements is also reported. The consequent adopted designs solutions are described together with the verification procedures. The verification process is presented through the description of experimental tests, data analysis and/or numerical simulations, which contributes all together to the assessment of the design soundness. The experimental tests often require the realization of ad hoc prototypes of different levels of complexity, e.g. the BB5 or the M4DP. The numerical analyses also imply the development of specific simulators, which can cover multi-disciplinary fields.

On one side the paper can furnish an overview of the typical development process of a complex system such as the E-ELT M4 deformable mirror, from the requirements generation to the design development, up to the system performance verification. On the other side, the paper shows the advanced status of the project, which is now in the final design phase and requires to refine and freeze all the design choices before launching the final production.

REFERENCES

[1] Biasi, R., Gallieni, D., Briguglio, R., Vernet, E., Andrighettoni, M., Angerer, G., Pescoller, D., Manetti, M., Tintori, M., Mantegazza, M., Lazzarini, P., Fumi, P., Anaclerio, V., Xompero, M., Pariani, G., Riccardi, A., Cayrel, M., Dierickx, P., Hubin, N., Kornweibel, N., Pettazzi, L., "E-ELT M4 Unit updated design and prototype results", [AO4ELT], (2015).

[2] Manetti, M., Morandini, M., Mantegazza, P., Biasi, R., Gallieni, D., & Riccardi, A., "Modeling and control of massively actuated, magnetically levitated, adaptive mirrors", [IEEE international conference on control applications], pp. 860–866, (2010).

[3] Quoilin, S., Bell, I., Desideri, A., Dewallef, P., Lemort, V., "Methods to Increase the Robustness of Finite-Volume Flow Models in Thermodynamic Systems", [Energies], 7, 1621-1640, (2014).

[4] Bell, I.H., Wronski, J., Quoilin, S., Lemort, V., " Pure and Pseudo-pure Fluid Thermophysical Property Evaluation and the Open-Source Thermophysical Property Library CoolProp", [Industrial & Engineering Chemistry Research], 53(6), (2014).

[5] Thome, J.R., [Engineering Data Book III], Wolverine Tube Inc, (2004).